Single-vehicle data of highway traffic: A statistical analysis

L. Neubert,[1,*] L. Santen,[1,2,†] A. Schadschneider,[2,‡] and M. Schreckenberg[1,§]
[1]*Theoretische Physik/FB 10, Gerhard-Mercator-Universität Duisburg, D-47048 Duisburg, Germany*
[2]*Institut für Theoretische Physik, Universität zu Köln, D-50937 Köln, Germany*
(Received 14 May 1999)

In the present paper, single-vehicle data of highway traffic are analyzed in great detail. By using the single-vehicle data directly, empirical time headway distributions and speed-distance relations can be established. Both quantities yield relevant information about the microscopic states. Several fundamental diagrams are also presented, which are based on time-averaged quantities and compared with earlier empirical investigations. In the remaining part, time-series analyses of the averaged as well as the single-vehicle data are carried out. The results will be used in order to propose objective criteria for an identification of the different traffic states, e.g., synchronized traffic. [S1063-651X(99)06712-4]

PACS number(s): 05.60.−k, 45.70.Qj, 45.70.Vn, 05.45.Tp

I. INTRODUCTION

Experimental and theoretical investigations of traffic flow have been the focus of extensive research interest during the past decades. Various theoretical concepts have been developed and numerous empirical observations have been reported (see, e.g., [1–25], and references therein). Despite these enormous scientific efforts, both theoretical concepts as well as experimental findings are still under debate. In particular, the empirical analysis turns out to be very subtle because the data strongly depend on several external influences, e.g., weather conditions or the performance of junctions [10]. Therefore, even certain experimental facts are not well established, although considerable progress has been made in the past few years. Recent experimental observations suggest the existence of three qualitatively different phases [11–14]: (i) *Free-flow states*, which are characterized by a large mean velocity, (ii) *synchronized states*, where the mean velocity is considerably reduced compared to the free-flow states, but all cars are moving, and (iii) *stop-and-go states*, where small jams are present. Synchronized traffic and stop-and-go states will be summarized as *congested states* in the following. Following Kerner [11], three different types of synchronized traffic exist. Long time intervals of constant density, flow, and velocity characterize the first type (i). In the second type (ii) variations of density and flow are observable, but the velocity of the cars is almost constant. Finally, there is no functional dependence between density and flow in the third type (iii) of synchronized traffic.

This work focuses basically on two points. First of all, we present a *direct analysis of single-vehicle* data which leads to a more detailed characterization of the different microscopic states of traffic flow, and second we use standard techniques of time-series analysis, i.e., utilization of autocorrelations and cross-correlations, in order to establish *objective* criteria for an identification of the different states.

A more detailed characterization of the microscopic structure of the different traffic states should lead to sensitive checks of the different modeling approaches. In particular, the time headway distributions and the speed-distance relations, which have been calculated from the single-vehicle data, allow for a quantitative comparison with simulation results of microscopic models [17,18]. Moreover, the objective criteria for an identification of the different traffic states, developed in the framework of this paper, enable us to perform an unbiased analysis of the experimental data.

The paper is organized as follows. In Sec. II we present some technical details of the given data set and of the measurements. The analysis of single-vehicle data is presented in Sec. III. Explicitly, we show results for the time headway distribution and the speed-distance relations. These results are compared to earlier estimates based on data from Japanese highways [19,20]. In Sec. IV we show the results for the fundamental diagram, i.e., the flow-density relation. Here we focus on the effect of different time intervals for the collection of data and discuss different methods of the calculation of the stationary fundamental diagram. Finally, the time-series analysis of the single-vehicle data as well as of the aggregated data is presented in Sec. V.

II. REMARKS ON THE DATA COLLECTION

The data set is provided by 12 counting loops all located at the German highway A1 near Cologne. At this section of the highway a speed limit of 100 km/h is valid — at least theoretically.

In Fig. 1 the section of the highway and the positions of the detectors are sketched. A detector consists of three individual detection devices, one for each lane. By combining three devices covering the three lanes belonging to one direction (except D2, see Fig. 1) one gets the cross sections labeled D1 through D4. The two detector arrangements D1 and D4 are installed nearby the intersection of two highways (AK Köln-Nord), while D2 and D3 are located close to a junction (AS Köln-Lövenich). These locations are approximately 9 km apart. In between there is a further junction but with a rather low usage. The most interesting results are obtained at D1, where the number of lanes is reduced from three to two for cars passing the intersection towards Köln-

*Electronic address: neubert@traffic.uni-duisburg.de
†Electronic address: santen@thp.uni-koeln.de
‡Electronic address: as@thp.uni-koeln.de
§Electronic address: shreck@traffic.uni-duisburg.de

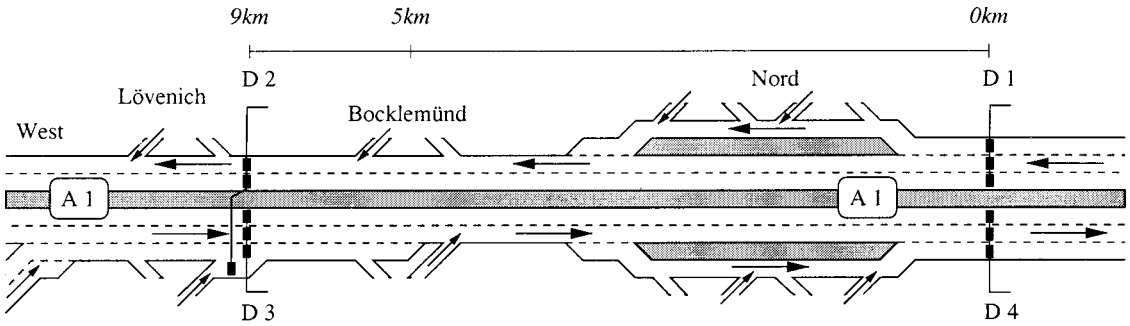

FIG. 1. Sketch of the analyzed section of the German highway A1. The arrows indicate the driving directions. The detector pairs D1-D4 and D2-D3 are about 9 km apart; in between, an additional junction is located.

Lövenich. Therefore, this part of the highway effectively acts as a bottleneck. Consequently, congested traffic is most often recorded at detector D1, and the analysis is based on this data set.

The data were collected between June 6, 1996 and June 17, 1996 when a total number of more than 500 000 vehicles passed each cross-section, nearly 16% of them being trucks and truck trailers. During this period the traffic data set was not biased due to road constructions or bad weather conditions.

The distance headway Δx as well as the velocity v of the vehicles passing a detector are collected in the data set. The velocity v is derived from the time elapsed between the crossing of the first and the second detector installed in a row with a known distance. The second direct measure is the time elapsed between two consecutive vehicles. Due to storage capacity reasons, only the time stamp with a rough resolution (only 1 sec) has been saved, but internally the high-resoluted time headway was used to determine the distance between the vehicle n and its predecessor $n-1$ via $\Delta x_n = v_{n-1}\Delta t_n$. This implies that the error in calculating Δx_n increases with Δt_n, since the calculation is made under the assumption of a constant speed v_{n-1}. It should be mentioned that this procedure gives correct results as long as the velocity of the vehicle which has passed the detector is constant until the following vehicle reaches the detector. So it is admissible to overcome the restriction of the resolution applying the reverse procedure to recover Δt_n with higher accuracy as it has been used in the framework of this paper.

For a sensible discussion it is plausible to split up the data set according to the different traffic states. In Fig. 2 a typical time series of one-minute aggregates of the speeds at the detectors D1 and D2 is shown. (Note: All shown figures which concern aggregated data use 1-min averaging intervals, if not mentioned otherwise. Flows and densities are measured per lane.) The transition from a free-flow to a congested state is indicated by a sudden drop of the local velocity. This allows for an undoubted separation of the data set into free-flow and congested regimes. The distinction between synchronized states, which were only of type (iii), and stop-and-go traffic was done using the cross-correlation (3) as described in Sec. V A. Then the analysis of the data has been performed separately for the free-flow and congested states excluding the transition regime. At D1, the most interesting installation, one obtains eight different periods of both free-flow and congested states. These periods are labeled by numbers I through VIII.

Figure 2 also shows the bottleneck effect given by the lane reduction near the intersection. At D1, the cross section behind the local defect, one gets a sudden drop in the velocity. On the other hand, downstream this cross section one finds only a weak decay of the velocity, which represents the outflow from a jam.

III. ANALYSIS OF SINGLE-VEHICLE DATA

In this section the results for the time-headway distributions and speed-distance relations calculated from single-vehicle data are presented. For a detailed examination the data set was classified in two ways. As mentioned above, a discrimination between free-flow and congested states was made, followed by a classification due to local densities. In Appendix A, it is described how the local density is deduced from the data set. Whereas the first one was done by a simple and manual separation by means of the time series of the speed, the second one requires a more detailed explanation: Every count belongs to a certain minute, and the local den-

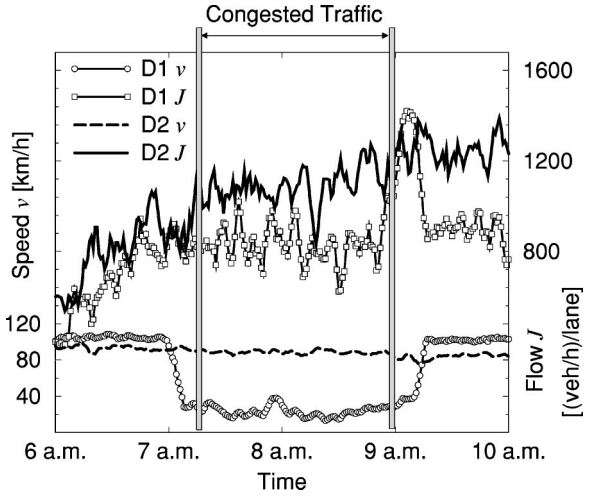

FIG. 2. Typical time series of flow and velocity. The transition from free to congested flow is indicated by a sharp fall of the average velocity. Upstream of the bottleneck one finds a strong reduction of the speed at D1, whereas the flow remains nearly constant. Downstream of the bottleneck at D2, the outflow from a jam is recorded — the speed is almost constant. It increases again after the jam at D1 has dissolved. For a proper characterization of the different states, we excluded the transition region, e.g., for the shown realization of a congestion we restricted our analysis on the part of the time series between the two vertical lines.

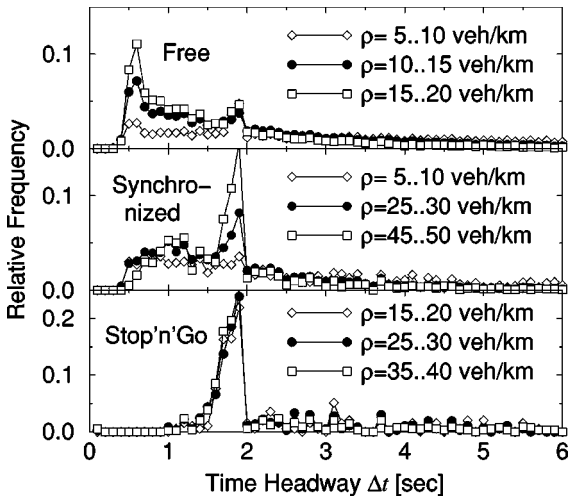

FIG. 3. Time headway distribution for different density regimes. Top: In free-flow traffic the Δt distribution is dominated by two peaks at 0.8 sec and 1.8 sec. Middle: In synchronized traffic, cars with narrow time gaps are found as well as a dominating peak. Bottom: In stop-and-go traffic, short time headways are suppressed. The peak at 1.8 sec remains since cars are leaving the jam with a typical temporal headway of approximately 2 sec.

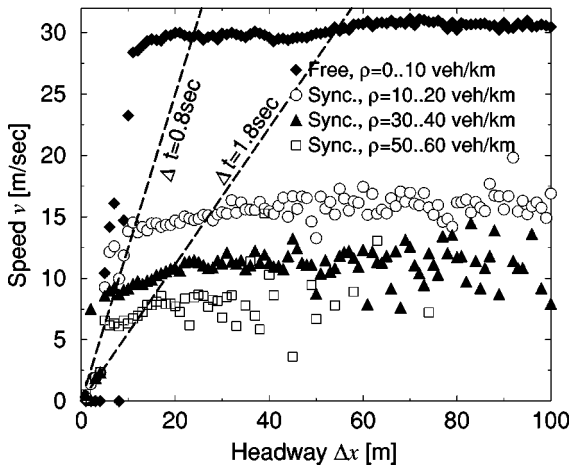

FIG. 4. The mean speed chosen by a driver depends on both the global traffic state and the gap between his predecessor. For a better orientation, the regions of characteristic temporal headways are also displayed.

sity ρ obtained during this certain minute is the criterion for the classification. That is, it is conceivable that a distance headway Δx is much larger than the mean distance headway $\langle \Delta x \rangle \propto \rho^{-1}$ of the considered period. Moreover, for the analyses made in this section a further distinction between synchronized states and stop-and-go traffic is necessary. This can be done using the cross-correlation (3) as described in Sec. V.

A. Time-headway distribution

So far, time-headway distributions have been investigated with regard to traffic composition or daytime [2,9]. The statistics were solely established on the basis of rather small data sets. A classification according to different traffic states, which will be presented in this section, was not used in earlier publications.

In Sec. II the way of calculating the time headways Δt_n is described in detail. In principle, the accuracy of the measurement would allow for a very fine resolution of the time headway distribution, but in order to obtain a reliable statistics we have chosen time intervals of length 0.1 sec.

In Fig. 3, the time-headway distributions of different traffic states at different local densities ρ are displayed. Regardless of the value of the local density, all free-flow distributions are dominated by a two-peak structure. The first peak at $\Delta t = 0.8$ sec represents the global maximum of the distribution and is in the range of time a driver typically needs to react to external incidents. On a microscopic level, these short time headways correspond to platoons of some vehicles traveling very fast — their drivers are taking the risk of driving ''bumper-to-bumper'' with a rather high speed. These platoons are the reason for the occurrence of high-flow states in free traffic. The corresponding states exhibit metastability, i.e., a perturbation of finite magnitude and duration is able to destroy such a high-flow state. Once such a collapse of the flow and the speed emerges, the free-flow branch can only be reached again by reducing the local density [21,22]. In the database considered here, such a sharp fall is not observable since all detected jams are caused by the bottleneck downstream of the detector D1. Additionally, a second peak emerges at $\Delta t = 1.8$ sec which can be associated with a typical drivers' behavior: It is recommended and safe to drive with a temporal distance of ≈ 2 sec corresponding to a maximum flow of ≈ 1800 vehicles/h.

Surprisingly, the small time headways have much less weight in congested traffic. Only the peak at $\Delta t = 1.8$ sec is recovered, where the time-headway distribution now takes the maximum value. But, nevertheless, the small time headways ($\Delta t < 1.8$ sec) contribute significantly in synchronized traffic. In stop-and-go traffic only the 1.8-sec peak remains and short time headways are suppressed. The asymptotic behavior is rather unsystematic and reflects the dynamics of vehicles inside the jams.

However, almost every fourth driver falls below the 1-sec threshold, and this is more likely when the traffic is free-flowing. Moreover, our results indicate that the small time headways are of the highest weight in the transition regime between free-flow and congested flow.

The common structure of the time-headway distributions in all density regimes can be summarized as follows: A background signal with exponential decay [2] covers a wide range of temporal headways, also for $\Delta t < 1$ sec. Additionally, at least one peak is to be noticed, whose location is independent of the underlying traffic state.

B. Speed distance-headway characteristics

Probably the most important information for an adjustment of the speed is the accessible distance headway Δx. This is captured by several models which use either a stationary fundamental diagram [23] or even more directly a so-called optimal-velocity (OV) function $v = v(\Delta x)$ as input parameters [20]. Therefore, a detailed analysis of the speed-distance relationship is of great importance for the modeling of traffic flow.

From Fig. 4 it is obvious that the average speed not only depends on Δx itself, but also on the local density. In par-

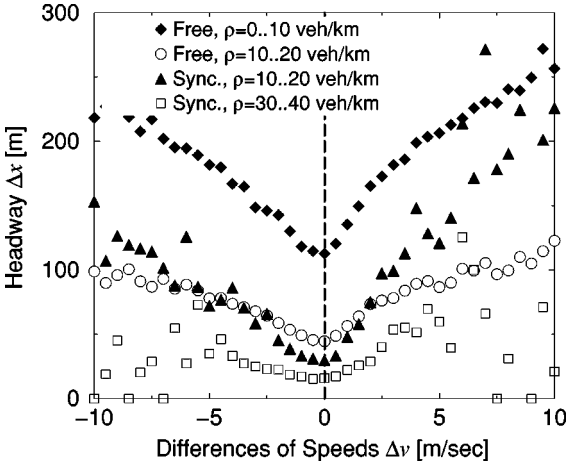

FIG. 5. The ''driving comfort'' is not decoupled from more ''technical'' features, i.e., vanishing differences of speed allow one to drive at the smallest mean distance headway.

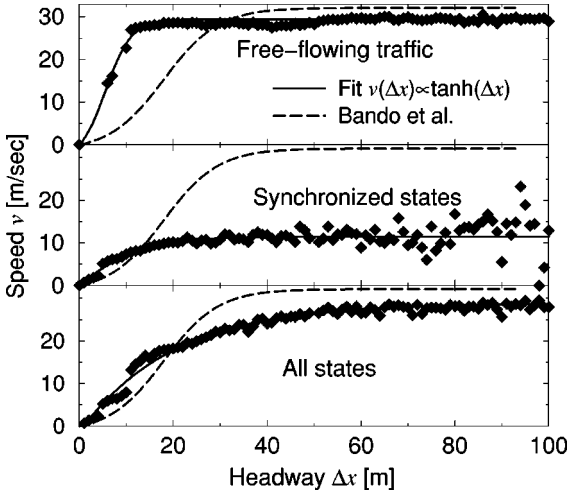

FIG. 7. Fits of the empirical data using the ansatz (1). The results are compared with the results given in [20].

ticular, the average speed for large distances in synchronized states is significantly lower than for the free-flow states, but also saturated for sufficiently large Δx. These observations should be relevant for theoretical approaches [24].

Next we also took into account the velocity differences $\Delta v_n = v_{n-1} - v_n$ between consecutive cars ($n-1$ followed by n). The dependence $\Delta x = \Delta x(\Delta v)$ is depicted in Fig. 5. The results clearly indicate that Δx is minimized if both cars move with the same velocity, irrespective of the microscopic state. Note that Δx is smaller than the mean distance derived from the inverse of the local density. Similar results and comparable conclusions were presented in [25], where the probability distribution $P(v_t - v_{t+\tau})$ was investigated. In this context v_t and $v_{t+\tau}$ are the speeds of two arbitrary but not necessarily consecutive vehicles crossing the detector with a temporal distance of τ seconds. They also observed a peak at $v_t - v_{t+\tau} = 0$ for any τ.

These observations are the motivation to determine an OV function using exclusively the data where $|\Delta v_n| \leqslant 0.5$ m/sec, because these should be relevant if an empirical OV function is demanded as input parameter for traffic models. By using this reduced data set, a better convergence of the OV function in the high-density regime is observable (Fig. 6). Nevertheless, at least the results in the free-flow and synchronized regimes strongly differ. This indicates that in synchronized traffic the drivers not only react to the distance of the vehicle ahead, they also take into account the situation at larger distances. It should be noticed that the dropping of measurements with $|\Delta v_n| > 0.5$ m/sec leaves only a fifth part of the data, but the quality of the OV diagrams does not suffer very much from this restriction.

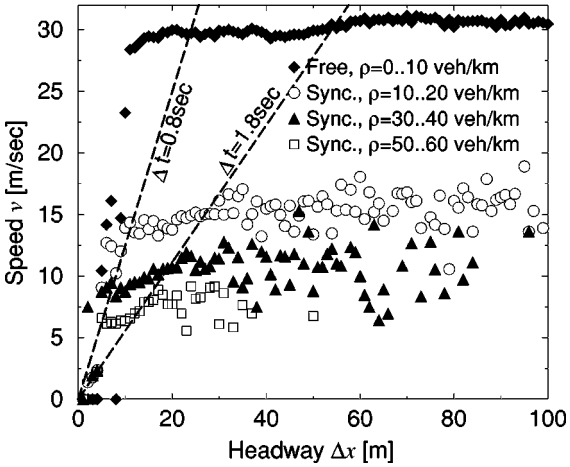

FIG. 6. If only vehicles with $|\Delta v_n| \leqslant 0.5$ m/sec are taken into account, the resulting OV function differs slightly from Fig. 4. Especially in the synchronized states, the measurements for $\Delta t \in [0.8\,\text{sec}, 1.8\,\text{sec}]$ are proportional to Δx; beyond $\Delta t = 1.8$ sec the data points are rather scattered.

In order to give explicit measures for the OV functions in the different density regimes, we used the ansatz

$$V(\Delta x) = k\{\tanh[a(\Delta x - b)] + c\} \tag{1}$$

suggested by Bando *et al.* [20], where a, b, c, k serve as fit parameters.

In Fig. 7 the empirical relations $v = v(\Delta x)$ are displayed averaging (top) over all states corresponding to free-flow, (middle) over all synchronized states, and (bottom) over all empirical data satisfying the restriction $|\Delta v_n| \leqslant 0.5$ m/sec. The comparison with an empirical OV function established by analyses of a car-following experiment on a Japanese highway [20] reveals a higher value of $V(\infty)$ and a slower increase of the OV function.

The characteristic values of the different OV functions are summarized in Table I, where D denotes the distance at which $V(D) = 0.95V(\infty)$ holds. The numerical results show

TABLE I. Characteristic parameters of the OV functions. The asymptotic values of the velocity $V(\infty)$ as well as the distance D, where 95% of $V(D)$ is exceeded (refer to Fig. 7).

	D	$V(\infty)$
Bando [20]	42.39	32.14
Free-flow (top)	14.11	29.43
Synchronized (middle)	26.70	11.47
All states (bottom)	57.70	28.64

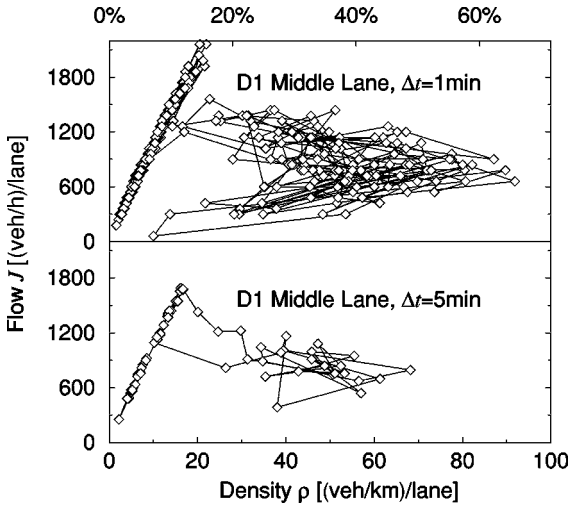

FIG. 8. Fundamental diagrams for different averaging intervals Δt. The upper diagram shows time-traced data averaged over $\Delta t = 1$ min while for the lower diagram $\Delta t = 5$ min has been used (for an explanation of the structure, see also Appendix A and Fig. 16). The relative occupation is calculated using the maximal density during the measuring period, $\rho_{\max} = 140$ vehicles/km.

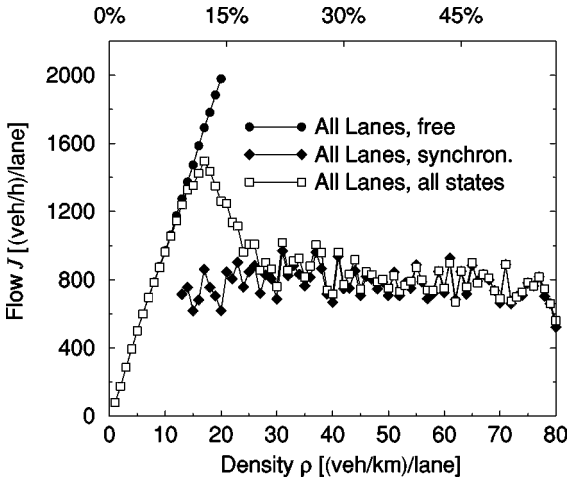

FIG. 9. Mean flow-density relation using the complete data set. The continuous curve corresponds to an average of all flow values for a given density while the discontinuous line is obtained discriminating between free-flow and synchronized states. Using the latter procedure, a nonunique behavior of the flow-density relation is observable which can also be seen near local defects in driven systems. Data points of the synchronized branch have been dropped for low densities due to the unreliable statistics.

that when averaging over both free-flow and congested states (Fig. 7, bottom) the asymptotic regime of the OV function is reached at much larger distances.

Our results for the OV functions can be summarized as follows. In the free-flow regime the functions are characterized by a steep increase at small distances corresponding to the small time headways discussed in the preceding subsection. For synchronized states it is remarkable that the asymptotic velocity takes a rather small value. Furthermore, our results show that it is necessary to distinguish between the traffic states in order to get a more precise description of the speed-headway relation.

IV. THE FUNDAMENTAL DIAGRAM

In this section we present results on the fundamental diagram based on time-averaged data. The present data set allows for a free choice of the averaging interval and overlaps. Here we compare the results obtained for one- and five-minute intervals (see also [1], p. 100). At the end of this section we discuss different methods in order to establish the stationary fundamental diagram.

In Fig. 8, fundamental diagrams for averaging intervals Δt of one and five minutes are shown. Beyond the trivial effect that longer averaging intervals lead to a reduction of the fluctuations, one observes that both the extremal values of the density and the flow decrease with growing Δt. Moreover, the small flow values at very low densities are averaged out if five-minute intervals are chosen. One might ask whether longer Δt's hide some real structure of traffic states or whether the additional structure in the one-minute intervals is a statistical artifact. From our point of view, the results for the low-density branch, which agree for both averaging intervals, indicate that a one-minute interval is sufficient to establish the systematic density dependence of the flow. Beyond that, microscopic states with short lifetimes can be detected using short time intervals, which makes the one-minute intervals preferable.

The unusual structure of the flow-density relation for small speeds, especially the return into the origin of the coordinate system, must be traced back to the method of the determination of the local density via J/v, since the occupation itself was not accessible in the underlying data set. This behavior will be explained in more detail in Appendix A.

In order to obtain the *stationary* flow-density relationship, we generated histograms from the fundamental diagram. Due to the problems of the density estimation in stop-and-go traffic, we omit these states in the further discussion. In Fig. 9 the results for two averaging procedures are displayed. The continuous form of the fundamental diagram has been obtained by averaging over all flow values of a given density, while the discontinuous shape has been obtained by discriminating between free-flow and synchronized traffic. It should be mentioned that the shape of the continuous stationary fundamental diagram also depends on the statistical weight of free-flow and synchronized states. Therefore, from our point of view it is necessary to distinguish between the different states in order to obtain reasonable results for the stationary fundamental diagram.

Using the latter method, it turns out that for high densities the average flow takes a constant value in a wide range of density. This plateau formation is similar to what is found by *global measurements* in driven systems with so-called impurity sites or defects, where in a certain density regime the flow is limited by the capacity of the local defect [26–29]. Here the bottleneck effect is produced by lane reduction as well as by the large activity of the on and off ramps at the intersection (see Sec. II).

V. TIME-SERIES ANALYSIS

As already mentioned in the Introduction, we propose *objective* criteria for the classification of different traffic states

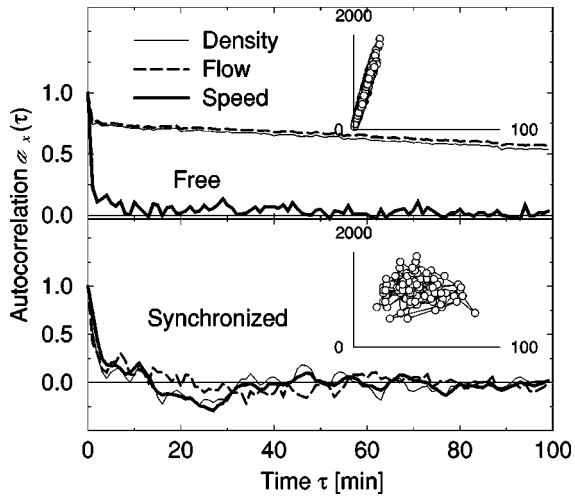

FIG. 10. Typical autocorrelation functions of the local density, the average velocity, and the flow in a free-flow (top) and synchronized (bottom) state. The insets show the fundamental diagram corresponding to the chosen time interval.

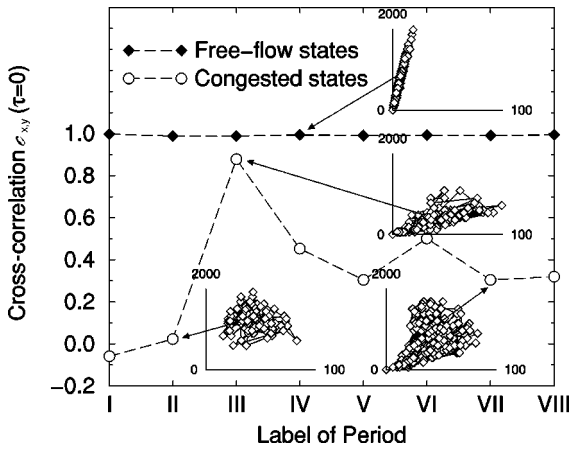

FIG. 11. Strong correlations between density and flow, indicated by $\varphi_{\rho,J}(0)\approx 1$, can be found in both free-flow and stop-and-go traffic. By contrast, synchronized states are characterized by weak correlations between density and flow. Congested states where transitions between synchronized and stop-and-go traffic appear lead to intermediate values of $\varphi_{\rho,J}(0)\approx 0.2,\ldots,0.5$. The different periods of free-flow and congested traffic are labeled by I through VIII (see also Sec. II). The dashed lines are a guide to the eyes only.

using standard methods of time-series analysis. Beyond that, we will show that these methods allow for a further characterization of the different states.

A. Correlation analyses

The first quantity to consider is the autocorrelation

$$\varphi_x(\tau)=\frac{\langle x(t)x(t+\tau)\rangle-\langle x(t)\rangle^2}{\langle x^2(t)\rangle-\langle x(t)\rangle^2} \tag{2}$$

of the aggregated quantities $x(t)$. The brackets $\langle\ \rangle$ indicate the average over a complete period of a free-flow or congested state.

In Fig. 10, the autocorrelations of one-minute aggregates of the density, flow, and average velocity of a free-flow and a synchronized state are shown. In the free-flow state the average speeds are only correlated on short time scales, whereas long-ranged correlations are present in the time series of local density as well as of the flow. This implies that no systematic deviations of the average velocity from the constant average value are observable, while the density and therefore also the flow vary systematically on much longer time scales up to the order of magnitude of hours. This long-range signal reflects the daily variation of the traffic loads.

This behavior of the autocorrelation is clearly contrasted with the behavior found in synchronized traffic, where *all* temporal correlations are short-ranged irrespective of the chosen observable. Both results show that longer time scales are only apparent in slow variations of the density during a day, while the other time series reveal a noisy behavior.

Furthermore, the cross-correlation

$$\varphi_{x,y}(\tau)=\frac{\langle x(t)y(t+\tau)\rangle-\langle x(t)\rangle\langle y(t+\tau)\rangle}{\sqrt{\langle x^2(t)\rangle-\langle x(t)\rangle^2}\sqrt{\langle y^2(t)\rangle-\langle y(t)\rangle^2}} \tag{3}$$

indicates the strong coupling between flow and density in the free-flow regime (Fig. 11). This implies that the variations of the flow are mainly controlled by density fluctuations while the average velocity is almost constant. Again the results for synchronized states differ strongly. Here all combinations of flow, density, and average velocity lead to small values of the cross-correlation also supporting the existence of irregular patterns in the fundamental diagram.

Therefore, the correlation analysis of the empirical data is in agreement with the interpretations given in [12,13], where synchronized states first have been identified. The synchronized states can be distinguished from stop-and-go traffic [14] using the same methods.

Similar to free-flow states, stop-and-go traffic is characterized by strong correlations between density and flow [$\varphi_{\rho,J}(0)\approx 1$]. The pattern in the flow density plane obtained during period III is quite similar to the patterns of synchronized states of type (ii). However, in this case a stop-and-go state is realized, which is indicated, e.g., by the small values of the speed. Beyond that, also the autocorrelation function shows an interesting behavior, namely an oscillating structure for all three quantities of interest (Fig. 12). The period of these oscillations is given by ≈ 10 min. This result is in accordance with measurements by Kühne [30], who found oscillating structures in stop-and-go traffic with similar periods.

The previous results allow us to establish the following objective criteria for the classification of traffic states: Free-flow and congested traffic can be distinguished using the time series of the mean speed, while the congested states differ with respect to the cross-correlation between densities and flow. In stop-and-go traffic, large values of the cross-correlation have been observed. The decoupling of density and flow in synchronized traffic is expressed through $\varphi_{\rho,J}(0)\approx 0$.

B. Transitions between the different states

These previous results show that the time-series analysis allows for an identification of different traffic states. Now we focus on the transition regime. Compared to the typical life-

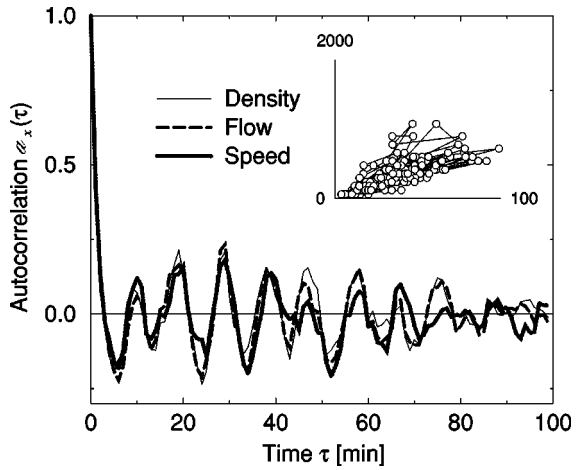

FIG. 12. The autocorrelations of all three local measures in stop-and-go traffic. All three local measures show oscillations around 0 with a period of ≈ 10 min.

time of a free-flow or a congested state, the transition is of short duration of approximately the order of magnitude of 15 min (see Fig. 13 for a typical time series of the local speed including a congested state).

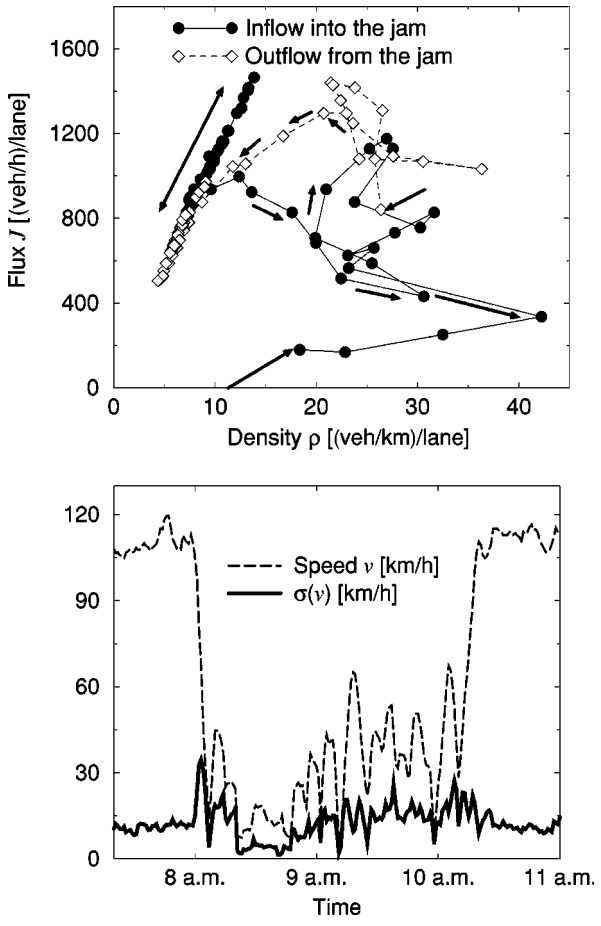

FIG. 13. Transitions between free-flow and congested traffic. The upper diagram shows one minute aggregates of the flow near a transition from free flow to a congested state and vice versa. For comparison, the time series of the one-minute aggregates of the local speed and their standard deviations are given in the diagram below.

Transitions from free-flow to both congested states are observable in the data set. The transitions take place at densities significantly lower than the density of maximum flow, since the transitions are initiated by a reduction of the capacity of the bottleneck and not by a continuous increase of the local density. We also want to mention that the congested states often are composed of stop-and-go and synchronized states, i.e., during a time series corresponding to congested traffic, transitions between both congested states frequently occur.

The results of several other empirical investigations suggest that the transition between free and congested flow is accompanied by a peak of the velocity variance at the transition [6,30]. Our analysis clearly does not support this result (see also [31]). The existence and height of the peak is closely related to the length of the averaging intervals. But of course these peaks are numerical artifacts. They show up because the time interval includes two different states but they do not reflect any further characteristics of the transition.

C. Correlation between different lanes

In addition to the irregular pattern in the fundamental diagram, it has been argued that a characteristic feature of the synchronized states is the strong coupling between different lanes [12,13]. These interpretations are mainly based on the fact that the average speeds on the different lanes approach one another. Here this effect is not observable because due to the speed limit even in the free-flow regime the average velocities on different lanes only slightly differ (the average speed in the free-flow regime in the left lane is given by ≈ 120 km/h and in the two other lanes by ≈ 100 km/h).

Therefore, we calculated $\varphi_{x_i,x_j}(\tau)$ in order to quantify this coupling effect. Here x_i denotes either the flow, the density, or the speed in lane i. In Fig. 14, the cross-correlations of different lanes belonging to the same driving direction are shown. The coupling between flow and density of neighboring lanes at $\tau=0$ in the synchronized state is comparable to the free-flow state. It is also apparent that the free-flow signal is veritable on long time scales, while in the synchronized state the correlation rapidly decays with time. Again this result mainly reflects the daily variation of the density.

The synchronization of the different lanes is indicated by large values $[\varphi_{v_i,v_j}(0)\approx 0.9]$ of the cross-correlation of the speed at $\tau=0$, while the time series of the speed on different lanes in free flow are completely decoupled.

D. Time series of the single-vehicle data

In the preceding section it could be shown that the relevant time scales are identifiable by time-series analyses. Here these methods, in particular a generalization of the cross-correlation function, will be used in order gain further information on the different microscopic states.

By using the single-vehicle data directly, it is not possible to evaluate the time dependence of $\varphi_x(t)$ in realistic units because the time intervals between consecutive signals strongly fluctuate. Instead of the temporal difference τ, now the number of cars n passing the detector between vehicle i and $j=i+n$ is used.

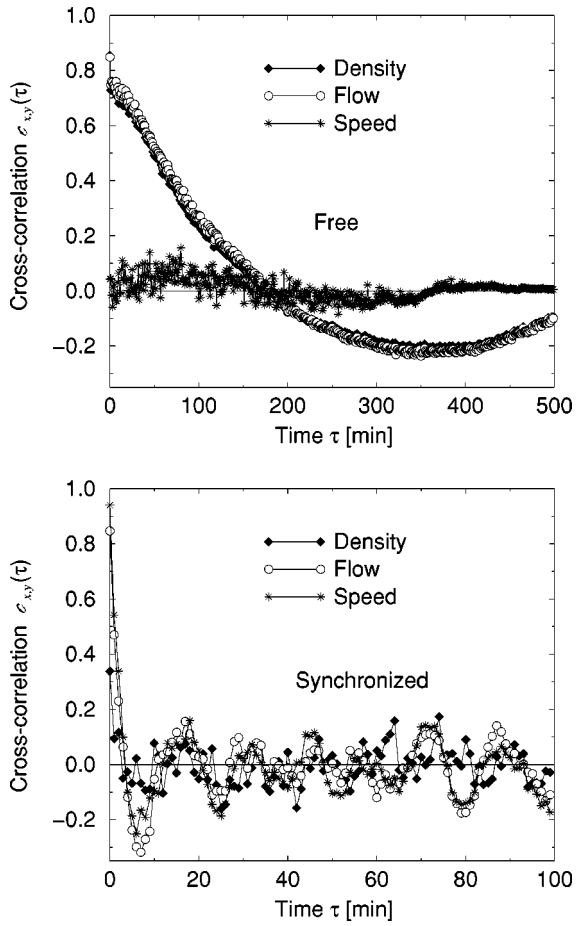

FIG. 14. Cross-correlation of flow, density, and speed of neighboring lanes in the free-flow regime compared to congested states. The shown data correspond to an average over all possible combinations of i and j.

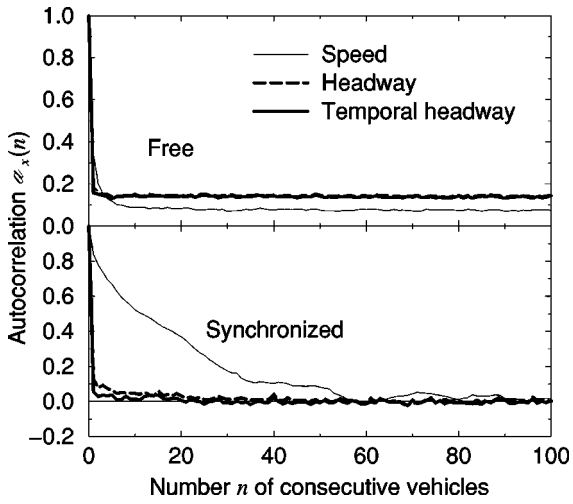

FIG. 15. A long-range signal is obtained from the autocorrelation of spatial and temporal headways among free-flowing vehicles (top). The diagram below is related to synchronized states and makes it clear that the correlations of the speeds are large on short scales (up to 50 vehicles), whereas that of the spatial and temporal headways decays very abruptly.

The behavior of the autocorrelation in the free-flow regime can be characterized as follows. For small n's one observes a steep decrease of $a_x(n)$ while an asymptotically slow decrease is found. The crossover from a fast to a slow decay has been observed for a small number of cars ($n \approx 5$).

In the free-flow regime, the single-vehicle data basically support the results obtained for the aggregated data, namely a strong coupling between the temporal headways (the single-vehicle analogy of the flow: $J \propto \Delta t^{-1}$) and the distances (corresponding to the density: $\rho \propto \Delta x^{-1}$). Moreover, the slow asymptotic decay is mainly due to the daily variation of the density. A different behavior has been found for $a_v(n)$. First the decay for small n is not as fast as for the other signals, and second the function decays faster asymptotically. The asymptotic behavior, in turn, is in accordance with the result drawn from aggregated data. But from our point of view the slower decrease for short distances is of special interest. It implies that also in the free-flow regime small platoons of few cars moving with the same speed are formed. These platoons lead to the peak at $\Delta t = 0.8$ sec in the time-headway distribution.

Having Fig. 15 in mind, $a_x(n)$ of synchronized state quantities behaves similarly, except for two differences: No long-ranged signal is present for all quantities of interest, and the decay of $a_v(n)$ for small n is much weaker than in the free-flow regime. This leads to the following picture of the microscopic states in synchronized flow: Similar to the free-flow regime, platoons are formed with cars moving at the same speed, but in synchronized flow these platoons are much larger (of the order of magnitude of some ten vehicles).

VI. SUMMARY AND CONCLUSION

In this paper a detailed statistical analysis of single-vehicle data of highway traffic is presented. The data allow us to analyze the microscopic structure of different traffic states as well as a discussion of time-averaged data.

Using the single-vehicle data directly, we calculated the time-headway distribution and the headway dependence of the velocity. Both quantities are of great interest for modeling of traffic flow, because they can be directly compared with simulation results [32] or are even used as input parameters [20] for several models.

Our analysis of the time-headway distribution has revealed a qualitative difference between the free-flow state and both congested states, i.e., synchronized traffic and stop-and-go traffic. The time-headway distribution of free-flow phases shows a two-peak structure. The first peak is located at very small time headways ($\Delta t \approx 0.8$ sec) while a second peak shows up at $\Delta t \approx 1.8$ sec. The peak at small time headways can be interpreted as a microscopic verification of metastable free-flow states. The second peak is also observed in congested flow. In synchronized states the small time headways, which contribute by the exponential underground, are still of statistical relevance. On the other hand, in stop-and-go traffic small time headways are strongly suppressed.

Similar results have also been obtained for the speed-distance relation, the so-called OV function [20]. It also turned out that it is necessary to distinguish between free-flow and synchronized states. In particular, the asymptotic velocities in free-flow and synchronized states differ

strongly. Moreover, a global average leads to different characteristics at small distances.

For comparison with earlier empirical investigations [12–14,31], we also have used aggregated data in order to calculate the fundamental diagram. Our results indicate that one-minute intervals are preferable compared to five-minute periods (the effect of different aggregation intervals has also been discussed in [6]), although these short intervals lead to larger fluctuations. Nevertheless, from our point of view, the single-vehicle data suggest that these fluctuations are not an artifact of the short averaging procedure but represent the complex structure of the different traffic states.

The data have also been used to calculate a stationary fundamental diagram. Again, our results reinforce that it is necessary to distinguish between free-flow and congested phases in order to get reliable results for the average flow at a given density. Then one obtains a discontinuous form of the fundamental diagram and a nonunique behavior of the flow in a density interval close to the density where the maximal flow is reached.

Using the autocorrelation and cross-correlation for the different time series, we were able to identify three qualitatively different microscopic states of traffic flow, namely the free-flow, synchronized, and stop-and-go traffic [11–14]. The free-flow states are characterized by a strong coupling of the flow and density and beyond that by a slow decay of the related autocorrelation functions. This implies that as far as a free-flow state is present, the flow solely depends on the density. The time scale which governs the asymptotic decay of the autocorrelation function is also determined by the daily variance of the density.

As shown in Sec. II, one can easily distinguish free-flow and congested states. By contrast, it is much more difficult to separate between time series belonging to stop-and-go and synchronized states by inspection. Therefore, an *objective* criterion is of great interest. It turns out that the time-series analysis provides such a criterion. Synchronized states are indicated by small values of the cross-correlation between flow, speed, and density. Moreover, the autocorrelation function is short-ranged for all three quantities. These results reflect the completely irregular pattern in the flow density plane [12,13] found for synchronized states. By contrast, in stop-and-go traffic, flow and density are strongly correlated. On the other hand, the autocorrelation function reveals an oscillating structure [30] with a period of the order of ten minutes. In addition, it was found that transitions between free-flow and congested flow are rare but transitions between the different congested states are more frequent.

The autocorrelation functions of the single-vehicle data have suggest that in the free-flow regime as well as in synchronized states, platoons of cars moving with the same velocity can be observed. Presumably, the platoons in the free-flow regime lead to the peak at $\Delta t \approx 0.8$ in the time-headway distribution and therefore to very large values of the flow.

From our point of view, our results have important implications for the theoretical description of traffic-flow phenomena. The short distance headways present in free-flow traffic are only possible when drivers anticipate the behavior of the vehicles in front of them [33]. Anticipation is less important in congested traffic. Another important effect is reflected by the gap dependence of the velocity at high densities. Here we observe a small asymptotic velocity. This implies that drivers tend to hold their speed in dense states, another feature which has to be captured by traffic models. Finally, one has to take into account the reduced outflow from a jam which has been verified by other authors and is supported by our results.

In conclusion, the analysis of single-vehicle data leads to a much better understanding of the microscopic structure of different traffic states. Although our results give a consistent picture of the experimental facts on highway traffic, an enlarged data set or data from other detector locations would be very helpful in order to settle the experimental findings. First of all, a series of counting loops would allow a more detailed analysis of the spatiotemporal structure of highway traffic, and additional data from on and off ramps would help to discriminate between bulk and boundary effects.

ACKNOWLEDGMENTS

It is our pleasure to thank B.S. Kerner and D. Chowdhury for fruitful discussions. The authors are grateful to the ''Landschaftsverband Rheinland'' (Cologne) for data support, to the ''Systemberatung Povse'' (Herzogenrath) for technical assistance, to the Ministry of Economic Affairs, Technology and Transport of North-Rhine Westfalia, as well as to the Federal Ministry of Education and Research of Germany for the financial support (the latter within the BMBF project ''SANDY'').

APPENDIX A

In principle, one could use the single-vehicle data directly in order to establish the velocity-flow relationship because the speed and the time headway (which is proportional to the inverse flow) of individual cars are provided by the detector. Unfortunately, an interpretation of these results is difficult because of the extreme fluctuations of the experimental data. Therefore, we used aggregated data in order to determine a fundamental diagram. In particular, we show the flow-density relationship of one- and five-minute aggregates.

While the local flow is directly given in the data set, one has to calculate the temporally averaged local densities ρ at the detector because the occupancy of a detector is not provided here. The occupancy of a detector denotes the fraction of time when the detector is occupied by vehicles. The local density can be calculated via the relation

$$\rho = J/v, \tag{A1}$$

where $J \propto N$ is closely related to the total number of cars N crossing the detector during the time interval $[t, t+\Delta t]$, and $v = \Sigma v_n(t)/N$ is the average velocity of the cars. Note that both the velocity $v_n(t)$ of the individual cars and the flow J are directly accessible. Therefore, this method should give the best estimate for the local density ρ as long as the velocity $v_n(t)$ represents a characteristic value of the local speed.

Problems using this kind of density calculation may arise from the strong fluctuations of the speed, especially in stop-and-go traffic. Then the velocity recorded by the detector gives a measure of the typical velocity of *moving* vehicles while the periods when cars do not move are not taken into account.

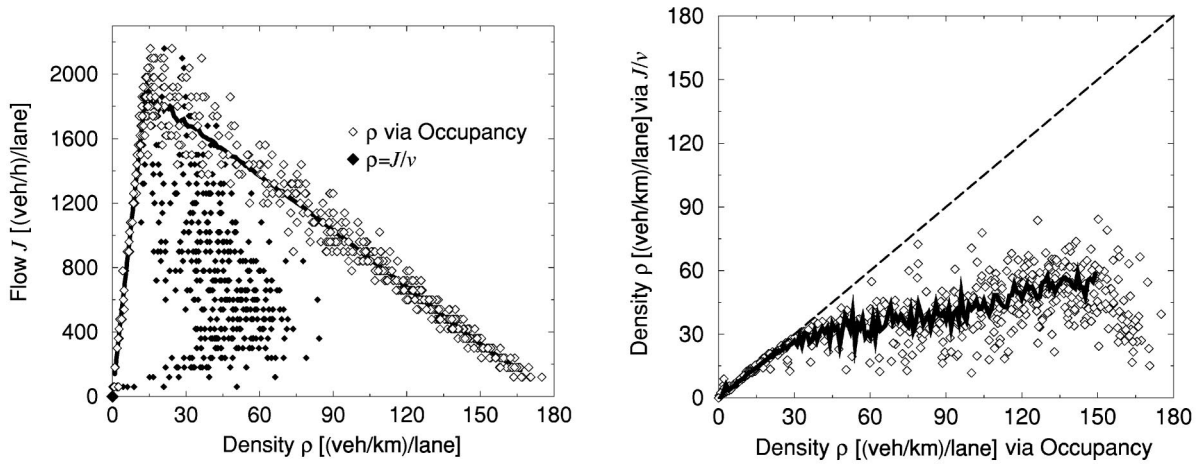

FIG. 16. Simulation results using different methods for the calculation of the local density. Top: The filled symbols correspond to an estimate calculated using Eq. (A1), while the open symbols represent the occupancy of the detector. Bottom: Comparison of both estimates. For $\rho>30$ vehicles/km, both methods strongly deviate from one another. Note that the density where these differences occur strongly depends on the chosen calibration of the model.

Figure 16 illustrates the effect of the different measuring procedures using computer simulations. During the simulation of a continuous version of the Nagel-Schreckenberg model (see Appendix B for a definition of the model), we used two kinds of detectors. The first detector is simply a line crosswise the driving direction. At this line, measurements of flows and velocities are performed. Then the local density is calculated via Eq. (A1). This result is compared with direct measurements of the local density where the average occupation on a short section of the lattice is detected. The figure shows that both estimates of the local density are in good agreement at low densities while at large densities the estimates may strongly differ. The different estimates for the local density lead to different shapes of the fundamental diagram. Estimating the density via the occupation of the detector, we get the well known form of a high-density branch while the calculation of the local density via Eq. (A1) leads to a pattern which is similar to free-flow states but with a much smaller average velocity.

Similar patterns have also been found in our data set (see Fig. 8). Therefore, the simulation results indicate that these periods correspond to stop-and-go traffic. Data points representing blocked cars are located in the origin of the fundamental diagram. Using an occupancy-based density, the points belonging to the same period would be shifted to the right. A deadlock situation would approach $(\rho_{\max},0)$, with $\rho_{\max}$ the maximum density. We suppose that $\rho_{\max}=140$ vehicles/km.

Finally, we want to mention that this problem cannot be circumvented using the speed-flow relation because one is still left with the problem of overestimating local speeds in stop-and-go traffic.

APPENDIX B

The simulation results have been obtained using a space-continuous version of the Nagel-Schreckenberg (NS) model [34,35] for single-lane traffic. Analogous to the NS model, the velocity of the nth car in the next time step is determined via the following four rules which are applied synchronously to all cars.

Step 1: Acceleration: $V_n \rightarrow \min(V_n+1, V_{\max})$.

Step 2: Deceleration (due to other vehicles): $V_n \rightarrow \min(V_n, d_n)$.

Step 3: Randomization: $V_n \rightarrow \max(V_n-\mathcal{A}(),0)$ with $\mathcal{A}() \in [0,1]$.

Step 4: Movement: $X_n \rightarrow X_n+V_n$.

The velocity of the nth car V_n is given in units of 5 m/sec. $V_{\max}$ denotes the maximum velocity, X_n the position of the cars, and $d_n=X_{n+1}-X_n-1$ the distance to the next car ahead. X_n and d_n are also given in units of 5 m (the length of the cars). $\mathcal{A}()$ is a random number between 0 and 1. In our simulation we use $V_{\max}=8$, which corresponds to 40 m/sec in realistic units.

The discrete NS model is also able to generate such fundamental diagrams, but with a worse resolution — the line of stop-and-go traffic has a rather steep slope. This is why we decided to use the continuous version of the NS model. Note that beside the better spatial resolution of the continuous version, no qualitative difference between the continuous and discrete version of the model has been found.

[1] H. Leutzbach, *Introduction to the Theory of Traffic Flow* (Springer, Berlin 1988).

[2] A.D. May, *Traffic Flow Fundamentals* (Prentice Hall, Englewood Cliffs, NJ, 1990).

[3] *Transportation and Traffic Theory*, edited by C.F. Daganzo (Elsevier, Amsterdam, 1993).

[4] *Traffic and Granular Flow*, edited by D.E. Wolf, M. Schreckenberg, and A. Bachem (World Scientific, Singapore, 1996).

[5] *Traffic and Granular Flow '97*, edited by M. Schreckenberg and D.E. Wolf (Springer, Singapore, 1998).

[6] D. Helbing, *Verkehrsdynamik* (Springer, Berlin, 1997).

[7] *Proceedings of the 14th International Symposium on Trans-*

portation and Traffic Theory, edited by A. Ceder (Pergamon, Amsterdam, 1999).
[8] *Traffic and Mobility: Simulation – Economics – Environment*, edited by W. Brilon, F. Huber, M. Schreckenberg, and H. Wallentowitz (Springer, Heidelberg, 1999).
[9] *Motorway Analysis: New Methodologies and Recent Empirical Findings*, edited by P.H.L. Bovy (Delft University Press, Delft, 1998).
[10] F.L. Hall, B.L. Allen, and M.A. Gunter, Transp. Res., Part A **20**, 197 (1986).
[11] B.S. Kerner, in [5], p. 239.
[12] B.S. Kerner and H. Rehborn, Phys. Rev. E **53**, R4275 (1996).
[13] B.S. Kerner and H. Rehborn, Phys. Rev. Lett. **79**, 4030 (1998).
[14] B.S. Kerner, Phys. Rev. Lett. **81**, 3797 (1998).
[15] H.Y. Lee, H.W. Lee, and D. Kim, e-print, cond-mat/9905292 (1999).
[16] J. Treiterer, Ohio State Technical Report No. PB 246094 (1975).
[17] D. Chowdhury, L. Santen, A. Schadschneider, S. Sinha, and A. Pasupathy, J. Phys. A **32**, 3229 (1999).
[18] A. Schadschneider, Eur. Phys. J. B **10**, 573 (1999).
[19] M. Koshi, M. Iwasaki, and I. Okuhra, in *Proceedings of the 8th International Symposium on Transportation and Traffic Theory*, edited by V.F. Hurdle, E. Hauer, and G.N. Steward (University of Toronto Press, Toronto, Ontario, 1983), p. 403.
[20] M. Bando, K. Hasebe, A. Nakayama, A. Shibata, and Y. Sugiyama, Jpn. J. Indust. Appl. Math. **11**, 203 (1994).
[21] B.S. Kerner and H. Rehborn, Phys. Rev. E **53**, R1297 (1996).
[22] R. Barlovic, L. Santen, A. Schadschneider, and M. Schreckenberg, Eur. Phys. J. B **5**, 793 (1998).
[23] B.S. Kerner and P. Konhäuser, Phys. Rev. E **48**, R2335 (1993).
[24] M. Treiber and D. Helbing, e-print, cond-mat/9901239 (1999).
[25] P. Wagner and J. Pleinke, Z. Naturforsch. A **52a**, 600 (1997).
[26] S.A. Janowsky and J.L. Lebowitz, Phys. Rev. A **45**, 618 (1992).
[27] G. Schütz, J. Stat. Phys. **71**, 471 (1993).
[28] Z. Csahok and T. Vicsek, J. Phys. A **27**, L591 (1994).
[29] D. Chowdhury, A. Pasupathy, and S. Sinha, Eur. Phys. J. B **5**, 781 (1998).
[30] R.D. Kühne, in *Proceedings of the 10th International Symposium on Transportation and Traffic Theory*, edited by N.H. Gartner and N.H.M. Wilson (Elsevier, New York, 1987), p. 119.
[31] D. Helbing, Phys. Rev. E **55**, R25 (1997).
[32] D. Chowdhury, A. Majumdar, K. Ghosh, S. Sinha, and R.B. Stinchcombe, Physica A **246**, 471 (1997).
[33] W. Knospe, L. Santen, A. Schadschneider, and M. Schreckenberg, Physica A **265**, 614 (1999).
[34] K. Nagel and M. Schreckenberg, J. Phys. I **2**, 2221 (1992).
[35] S. Krauß, P. Wagner, and C. Gawron, Phys. Rev. E **54**, 3707 (1996).